


## Article

# Sorption of Acridine Orange on Non-Swelling and Swelling Clay Minerals

Wei-Teh Jiang <sup>1,\*</sup>, Yolin Tsai <sup>1</sup>, Xisen Wang <sup>2</sup>, Hannah J. Tangen <sup>3</sup>, Jessica Baker <sup>4</sup>, Lori Allen <sup>3</sup> and Zhaohui Li <sup>4,\*</sup> 

<sup>1</sup> Department of Earth Sciences, National Cheng Kung University, 1 University Road, Tainan 70101, Taiwan; yolintsai@hotmail.com

<sup>2</sup> Department of Chemistry, California State University, Sacramento, CA 95819, USA; x.wang@csus.edu

<sup>3</sup> Department of Chemistry, University of Wisconsin–Parkside, 900 Wood Road, Kenosha, WI 53144, USA; tange002@rangers.uwp.edu (H.J.T.); allen@uwp.edu (L.A.)

<sup>4</sup> Department of Geosciences, University of Wisconsin–Parkside, 900 Wood Road, Kenosha, WI 53144, USA; baker064@rangers.uwp.edu

\* Correspondence: atjw@mail.ncku.edu.tw (W.-T.J.); li@uwp.edu (Z.L.)

**Abstract:** Acridine orange (AO) is a cationic fluorescent dye commonly used in DNA analyses. Extensive studies were conducted for its metachromasy under different solution concentrations and different amounts of AO sorbed on a solid surface. Meanwhile, for the safe disposal of wastewater, AO removal from water using different materials was also evaluated extensively. Clay minerals, due to their large specific surface area, high cation exchange capacity, and vast reserves, have been evaluated as potential sorbents for the removal of a variety of different types of contaminants, including color dyes. In this study, the sorption of AO on different types of clay minerals was contrasted. The sorption of co-presenting  $\text{Zn}^{2+}$  was much less than the sorption of AO, suggesting that clay minerals have higher affinities for AO in comparison to inorganic  $\text{Zn}^{2+}$ . The desorption of exchangeable cations was linearly related to AO sorption, and the amounts of AO sorbed were close to the CEC values of the minerals, confirming that cation exchange is the dominating mechanism for AO sorption. Molecular dynamics simulation results showed that, under low and high AO loading levels, the sorbed AO formed monolayers and bilayers on the mineral surfaces of non-swelling clay minerals, except halloysite, as well as in the interlayer of swelling clay minerals, due to its relatively large dimer constant in solution. Overall, clay minerals are good candidates for the removal of cationic dyes from solution even in the presence of competing inorganic cations.

**Keywords:** acridine orange; cationic dye; cation exchange; clay; co-presenting cation; sorption; mechanism



**Citation:** Jiang, W.-T.; Tsai, Y.; Wang, X.; Tangen, H.J.; Baker, J.; Allen, L.; Li, Z. Sorption of Acridine Orange on Non-Swelling and Swelling Clay Minerals. *Crystals* **2022**, *12*, 118. <https://doi.org/10.3390/cryst12010118>

Academic Editor: Vladislav V. Gurzhiy

Received: 16 December 2021

Accepted: 13 January 2022

Published: 17 January 2022

**Publisher's Note:** MDPI stays neutral with regard to jurisdictional claims in published maps and institutional affiliations.



**Copyright:** © 2022 by the authors. Licensee MDPI, Basel, Switzerland. This article is an open access article distributed under the terms and conditions of the Creative Commons Attribution (CC BY) license (<https://creativecommons.org/licenses/by/4.0/>).

## 1. Introduction

Acridine orange (AO) is a cationic fluorescent dye commonly used in DNA analyses [1]. As such, early studies were focused on its metachromasy after its sorption or intercalation into montmorillonite (MT) minerals [2–4]. AO sorption on Wyoming MT was attributed to cation exchange, and different exchangeable cations resulted in different amounts of AO sorption in the order  $\text{Na} > \text{H} > \text{Cu} > \text{Mg} > \text{Al}$  at the values of 1, 0.9, 0.9, 0.87, and 0.55 mmol/g [2]. In addition, AO sorption capacities on saponite and Na-beidellite were 2 and 3 mmol/g, much larger than their cation exchange capacity (CEC) of 0.78 and 1.09 mmol<sub>c</sub>/g, with hydrophobic interactions being attributed to the AO sorption above the CEC values [3,4]. Similarly, acridine sorption on hectorite and another saponite reached 1.4 mmol/g, in comparison to CECs of 0.89 and 0.80 mmol<sub>c</sub>/g [5]. More recently, in one study, AO sorption on SWy-2 (Na-MT) and SHCa-1 (Li-bearing trioctahedral smectite) reached a capacity of 1.2 mmol/g, much higher than the CEC values of 0.85 and 0.66 mmol<sub>c</sub>/g [6]. Proportional desorption of exchangeable cations from expandable clay minerals accompanying AO sorption suggested cation exchange as the most dominant

mechanism [6]. Furthermore, on SAz-1 (a Ca-MT), AO sorption reached a capacity of 1.6 mmol/g, which is 30% higher than its CEC value, and cation exchange was considered the dominant mechanism at low AO loading levels up to 0.8 mmol/g, beyond which molecular association into a horizontal bilayer formed in the interlayer of MT [7]. A raw and a purified clay with CEC values of 0.6 and 1.1 mmol<sub>c</sub>/g made of smectite and kaolinite showed AO sorption of 0.6 and 1 mmol/g, and the sorption of AO involved AO intercalation [8]. A laponite was studied for AO dimer formation on its surface, and the dimers increased with more AO loading up to 50% of its CEC value, but the location of the AO on the surface or in the interlayer was not mentioned [9]. In these studies, the AO used was in HCl form without co-presenting divalent cation Zn<sup>2+</sup>. However, for commercially available AO dyes, one will have ZnCl<sub>2</sub> in the formula.

In addition to clay minerals, extensive studies were also conducted on AO removal from water using different types of sorbents including ZnO/graphene oxide [10], layered double hydroxides (LDHs) [11], and magnetic nano  $\gamma$ -Fe<sub>2</sub>O<sub>3</sub> particles [12]. AO sorption was studied using ZnO/graphene oxide, but the influence of Zn on AO sorption was not mentioned [10]. Similarly, AO sorption on a zinc oxide/almond shell activated carbon composite was investigated, but the influence of ZnO on enhancing AO sorption was not discussed [13].

The enhancement of AO fluorescence under the influence of clay minerals was another topic of study. UV/Vis absorption and fluorescence emission spectra of 2:1 layered clay minerals montmorillonite (MT), rectorite (RT), and illite (IT) loaded with different amounts of AO showed that, under low loading levels, maximal AO fluorescence could be achieved, as the dye molecules could be primarily located on the external surfaces of the platy minerals with optimal dye molecule separation, and that, under high loading levels, extensive quenching happened as the sorbed AO molecules could form multilayers on the surface or bilayers in the interlayer [14]. Similarly, AO sorption on 1:1 layered clay minerals kaolinite (KAO) and halloysite (HAL) also showed the same fluorescence effect [15]. However, a systematic assessment using different types of clay minerals for sorptive removal of AO from solution was limited.

In this study, the sorption of AO on non-swelling and swelling clay minerals was conducted. The AO sorbed clay minerals were characterized by X-ray diffraction (XRD) and Fourier-transform infrared (FTIR) analyses. The desorption of exchangeable cations was monitored by ICP analyses. According to the amount of AO and Zn<sup>2+</sup> sorbed, the surface or interlayer configuration of AO and Zn<sup>2+</sup> was subjected to molecular dynamics simulation. The objective of the study was to contrast the AO sorption sites and sorption mechanisms on non-swelling and swelling clay minerals, so that proper selection could be achieved when using clay minerals as sorbent for the removal of cation dyes.

## 2. Materials and Methods

### 2.1. Materials

The color dye AO was obtained from Alfa Aesar with a formula of C<sub>17</sub>H<sub>19</sub>N<sub>3</sub>·HCl·ZnCl<sub>2</sub>, a molecular weight of 438.1 g/mol, a CAS # of 10127-02-3, and a pK<sub>a</sub> value of 10.4 [16]. It has molecular dimensions of 1.304 nm length by 0.590 nm width by 0.388 nm thickness (Figure 1a). Its chemical structure and pH speciation are illustrated in Figure 1. Its isosbestic point at 470 nm [17] occurs at concentrations of 1–5 × 10<sup>−5</sup> M [18].

The non-swelling clay minerals used were KGa-1b well-crystallized kaolinite (KAO), halloysite (HAL), and IMt-2 illite (IT). The swelling clay minerals used were SAz-2, Ca-montmorillonite (MT), and rectorite (RT). The HAL was purchased from Sigma-Aldrich, while the RT was obtained from Zhongxiang, Hubei, China. The remaining minerals were obtained from the Source Clay Minerals Repository (Purdue University, West Lafayette, IN, USA). The reported CEC values were 0.03 mmol<sub>c</sub>/g for KAO [19], 0.115 mmol<sub>c</sub>/g for HAL [20], 1.25 and 0.147 mmol<sub>c</sub>/g for MT and IT [21], and 0.44 mmol<sub>c</sub>/g for RT [22]. Meanwhile, the specific surface area (SSA) values were 13.1 and 65 m<sup>2</sup>/g for KAO and HAL [20], and 84, 20, and 20 m<sup>2</sup>/g for MT, RT, and IT, respectively [14].

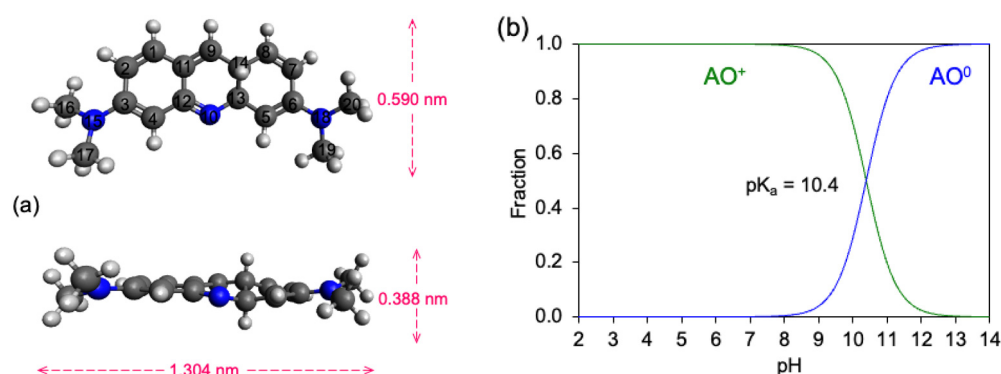


**Figure 1.** Molecular structure of AO with its dimensions (a) and its pH speciation diagram (b).

## 2.2. AO Sorption Experiments

As AO is a cationic dye and the sorption of AO on negatively charged mineral surfaces occurs via the cation exchange process, the amount of clay mineral and the initial concentrations of OA used were dependent on the CEC values of the minerals. The amount of solid used was 0.1 g, and the volume of solution used was 30 mL. For MT, the initial concentrations were 1, 2, 4, 6, 8, and 10 mmol/L due to its high cation exchange capacity, while, for all other minerals, the initial concentrations of 0.5, 1, 2, 3, 4, and 5 mmol/L were used. They were shaken in a horizontal way with end-over-end shaking direction on a shaker table for 24 h at 150 rpm, centrifuged for 10 min at 5000 rpm, and then filtered with 0.45  $\mu\text{m}$  syringe filters before being analyzed for equilibrium AO concentration using a UV/Vis method at the wavelength of 490 nm and for  $\text{Zn}^{2+}$  concentration by ICP.

## 2.3. Instrumental Analyses

As the AO solid contains  $\text{Zn}^{2+}$ , equilibrium  $\text{Zn}^{2+}$  concentrations were analyzed using an ICP-OES apparatus (Optima 7000 DV) made by Perkin Elmer. At the same time, desorption of exchangeable cations  $\text{K}^+$ ,  $\text{Na}^+$ ,  $\text{Ca}^{2+}$ , and  $\text{Mg}^{2+}$  was also analyzed by ICP-OES. The XRD analyses were conducted using a Bruker D8A Advance X-ray diffractometer with  $\text{CuK}\alpha$  radiation at 40 kV and 40 mA and a scanning speed of  $1^\circ/\text{min}$  or a Shimadzu 6100 X-ray diffractometer with an Ni-filtered  $\text{CuK}\alpha$  radiation at 30 kV and 40 mA and a scanning speed of  $2^\circ/\text{min}$ . Samples were scanned from  $2$ – $32^\circ$  ( $2\theta$ ). Oriented samples were used to investigate the expansion of (001) reflections for the swelling clay minerals. The FTIR spectra were acquired on a Shimadzu 8100 spectrometer equipped with a quartz ATR. Samples were scanned from  $400$  to  $4000\text{ cm}^{-1}$  with a resolution of  $2\text{ cm}^{-1}$ .

## 2.4. Molecular Dynamics Simulations

Molecular simulations were performed using the ‘FORCITE’ module in Materials Studio 6.0 software to determine the surface or interlayer configuration of sorbed AO molecules and the location of co-sorbed  $\text{Zn}^{2+}$ . The supercells were built on the basis of the SSA, the unit-cell parameters of each mineral, and the amounts of AO sorbed on each mineral at different loading levels. For KAO and HAL, the super cells were made of  $4a \times 4b$  with the AO sorption capacities of 0.055 and 0.12 mmol/g, respectively, under which 16 molecules and four  $\text{Zn}^{2+}$  cations or seven AO molecules and two  $\text{Zn}^{2+}$  cations would sorb on the supercell according to their CEC and SSA values. The AO sorption was also simulated at the CEC value of 0.03 mmol<sub>c</sub>/g, under which eight AO molecules and two  $\text{Zn}^{2+}$  cations were used per KAO super cell.

For IT, MT, and RT, the supercell was made using  $3a \times 3b$  unit cells. For IL under the low and high loading levels, three and six AO molecules and one and two  $\text{Zn}^{2+}$  cations were used. For MT and RT, one and two AO molecules were used for the low loading level, and six and five molecules were used for the high loading level. Meanwhile, zero or one  $\text{Zn}^{2+}$  was used under these conditions. For MT, the total surface area of  $760\text{ m}^2/\text{g}$  [23] was used for determination of the number of AO molecules. For RT, a total surface area

of 200 m<sup>2</sup>/g was used as it is a swelling clay mineral and AO intercalation occurred extensively according to XRD analyses, even though the SSA value was only 20 m<sup>2</sup>/g. The simulation was performed for sorption at 298 K, and the constructed model was optimized geometrically.

### 3. Results

#### 3.1. AO Sorption

The sorption of AO, Zn<sup>2+</sup>, and AO + Zn<sup>2+</sup> on non-swelling clay minerals KAO, HAL, and IT is plotted in Figure 2, and all cases followed the Langmuir sorption model, expressed as

$$C_s = \frac{K_L S_m C_L}{1 + K_L C_L} \quad (1)$$

where  $C_L$  and  $C_s$  are the AO concentration in solution (mmol/L) and amount of AO sorbed (mmol/kg) on the minerals at equilibrium, while  $S_m$  (mmol/kg) and  $K_L$  (L/mmol) are the Langmuir parameters reflecting the AO sorption capacity on and affinity for the minerals.

The Langmuir equation can be rearranged into a linear form so that  $S_m$  and  $K_L$  can be determined linearly.

$$\frac{C_L}{C_s} = \frac{1}{K_L S_m} + \frac{C_L}{S_m} \quad (2)$$

For the non-swelling clay minerals, the calculated sorption capacities of AO, Zn<sup>2+</sup>, and AO + Zn<sup>2+</sup> were 0.055, 0.015, and 0.07 mmol<sub>c</sub>/g on KAO, 0.12, 0.04, and 0.16 mmol<sub>c</sub>/g on HAL, and 0.09, 0.07, and 0.16 mmol<sub>c</sub>/g on IT (Figure 2a–c). The CEC values were 0.030 mmol<sub>c</sub>/g for KAO [19], 0.115 mmol<sub>c</sub>/g for HAL [20], and 0.15 mmol<sub>c</sub>/g for IT. For KAO, the AO sorbed alone was almost twice its CEC value; however, for HAL and IL, the AO sorbed alone was less than their CEC values (Table 1). In contrast, for KAO, the AO + Zn<sup>2+</sup> sorbed was about twice its CEC value. For HAL, the AO + Zn<sup>2+</sup> was 30% more than its CEC value. For IL, AO + Zn<sup>2+</sup> sorbed was similar to its CEC value. These results suggested that, at the AO sorption capacities, the amount of Zn<sup>2+</sup> sorbed contributed to 20–45% of the total cations sorbed in mmol<sub>c</sub>/g.

The results strongly suggest that cation exchange played an important role in AO sorption on these clay minerals. A previous report showed that AO sorption on Na-beidellite resulted in a proportional release of metallic cations from the mineral into the aqueous solution [24]. To further confirm the cation exchange mechanism, the release of metal cations was monitored in the isotherm study. The desorption of exchangeable cations K<sup>+</sup>, Na<sup>+</sup>, Ca<sup>2+</sup>, and Mg<sup>2+</sup> was proportional to the amount of AO + Zn<sup>2+</sup> sorbed with slopes of 1.3, 0.8, and 1.4 for KAO, HAL, and IT (Figure 2d–f). These results confirmed that cation exchange was the dominating mechanism of AO sorption on non-swelling clay minerals.

Similarly, the AO, Zn<sup>2+</sup>, and AO + Zn<sup>2+</sup> sorption on swelling clay minerals also followed the Langmuir isotherm with capacities of 1.15, 0.46, and 1.60 mmol<sub>c</sub>/g on MT and 0.40, 0.20, and 0.60 mmol<sub>c</sub>/g on RT (Figure 3a,b). The amount of Zn<sup>2+</sup> sorbed accounted for one-third of the total cation sorbed and about 30–50% of the AO sorbed (Table 1). The results for AO + Zn<sup>2+</sup> sorption are in agreement with a previous AO sorption capacity of 1.6 mmol/g on SAz-1 [7], whose CEC value was 1.25 mmol/g [2]. For Wyoming MT, whose CEC value was 0.87 mmol/g [2], the AO sorption capacity was up to 1.35 mmol/g [2]. However, the AO used in these studies was in HCl form and Zn<sup>2+</sup> was not present. For RT, its CEC value was 0.44 mmol<sub>c</sub>/g. For the swelling clay minerals, the sorption of AO + Zn<sup>2+</sup> was 25% to 30% more than the CEC of MT and RT. Similarly, for Na-beidellite, AO sorption could be as high as 3 mmol/g, and the AO sorption beyond the CEC value was attributed to hydrophobic interaction [24]. Desorption of exchangeable cations K<sup>+</sup>, Na<sup>+</sup>, Ca<sup>2+</sup>, and Mg<sup>2+</sup> was also proportional to the amount of AO + Zn<sup>2+</sup> sorbed with slopes of 1.1 and 1.0 for MT and RT, respectively (Figure 3c,d). These results confirmed that cation exchange was also primarily responsible for AO sorption on swelling clay minerals. To independently confirm the sorption of Zn<sup>2+</sup> on the mineral surface, electron microprobe

analyses were performed for KAO and HAL. Indeed, a minute Zn peak showed up for both minerals at high AO loading levels (Figure 4).

**Table 1.** AO or AO + Zn<sup>2+</sup> sorption capacity on different types of clay minerals.

Clay Minerals	KAO	HAL	IT	MT	RT
S <sub>m</sub> (mmol/g) for AO	0.055	0.12	0.09	1.15	0.40
S <sub>m</sub> (mmol <sub>c</sub> /g) for AO + Zn <sup>2+</sup>	0.07	0.16	0.16	1.60	0.60
CEC (mmol <sub>c</sub> /g)	0.03	0.115	0.15	1.25	0.44

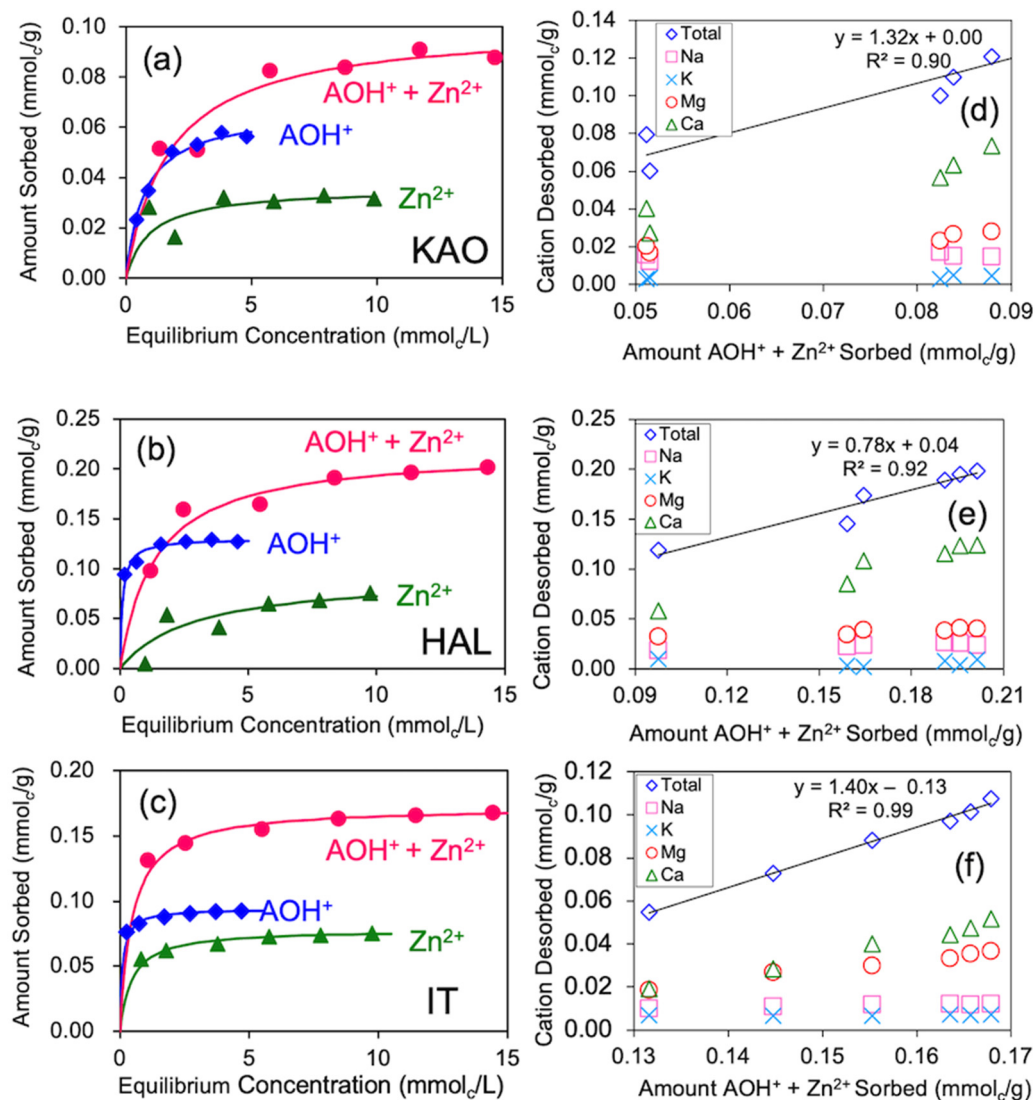


**Figure 2.** Sorption isotherms of AO on KAO (a), HAL (b), and IT (c); desorption of exchangeable cations from KAO (d), HAL (e), and IT (f) accompanying AO sorption. As the molarity of Zn to AO was 1:1 in solution and Zn has a charge of 2+, the Zn<sup>2+</sup> sorbed and total AO + Zn<sup>2+</sup> sorbed are also plotted in these figures to show the stoichiometric of cation exchange.



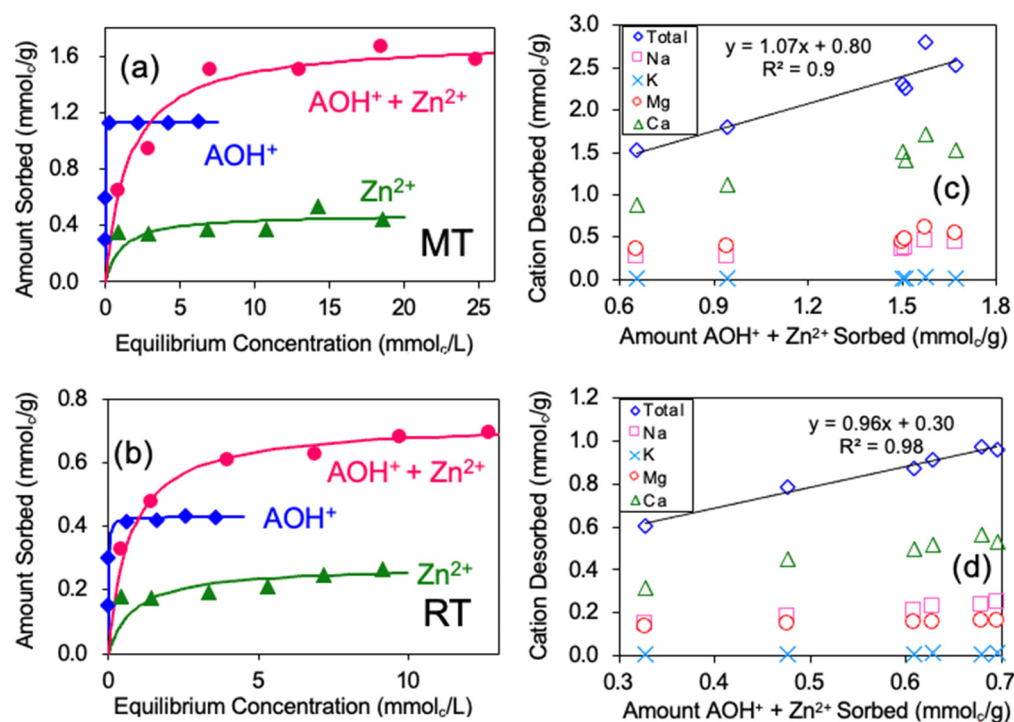


**Figure 3.** Sorption isotherms of AO on MT(a) and RT (b), and the desorption of exchangeable cations from MT (c) and RT (d) accompanying AO sorption. As the molarity of Zn to AO was 1:1 in solution and Zn has a charge of 2+, the Zn<sup>2+</sup> sorbed and total AO + Zn<sup>2+</sup> sorbed are also plotted in these figures to show the stoichiometric of cation exchange.

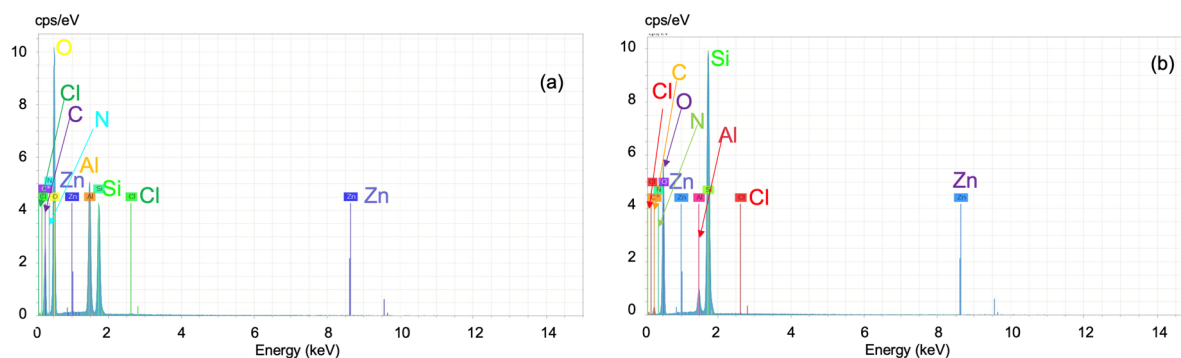


**Figure 4.** EDS spectra showing the presence of Zn<sup>2+</sup> on the surface of KAO (a) and HAL (b).

### 3.2. XRD Analyses

The XRD results of non-swelling clay minerals after sorption of different amounts of AO are illustrated in Figure 5. For HAL, although the crystallinity is low, the first peak showed that it is a 7 Å halloysite. Regardless of the amount of AO sorbed, there was no change in d-spacing for any of the visible peaks, indicating that the location of the AO or AO + Zn<sup>2+</sup> sorption was on the external surfaces.

For swelling clay minerals MT and RT, the  $d_{001}$  spacing increased as the amount of AO sorption increased, suggesting that more AO or AO + Zn<sup>2+</sup> sorption occurred in the interlayer space at high AO sorption levels (Figure 6). For Na-MT,  $d_{001}$  increased from 1.28 to 1.58 nm at an AO input of 0.1 M/100 g clay [4]. For virgin Na-beidellite, after heating to 110 and 300 °C, the  $d_{001}$  spacing collapsed to 1.0 nm, whereas, for AO intercalated beidellite, no decrease in  $d_{001}$  occurred after heating, indicating that the sorbed AO was at the interlayer of beidellite [24].

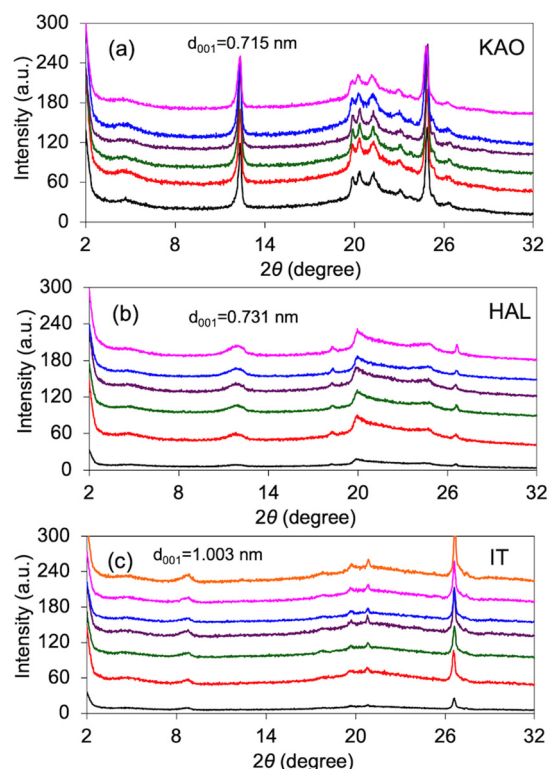


**Figure 5.** XRD patterns of KAO (a), HAL (b), and IT (c) showing no expansion of any peaks after sorption of AO. From bottom up, the initial AO concentrations were 0, 1, 2, 3, 4, and 5 mM.

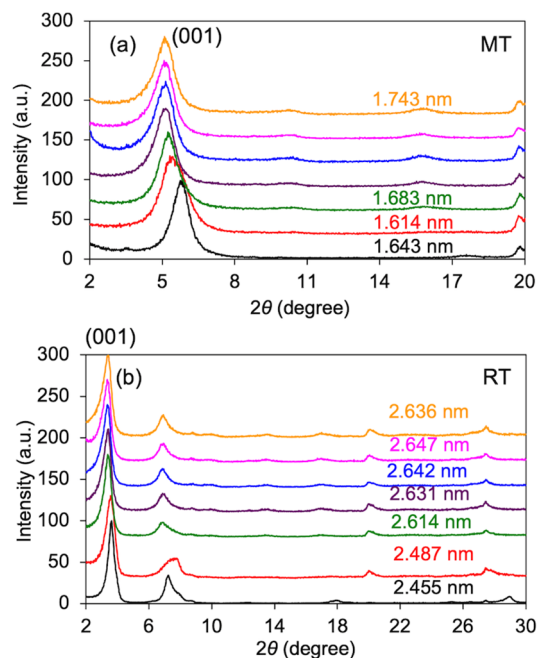


**Figure 6.** XRD patterns of MT (a) and RT (b) showing the expansion of (001) after sorption of AO. From bottom up, the initial AO concentrations were 0, 1, 2, 4, 6, 8, and 10 mM for MT and 0, 0.5, 1, 2, 3, 4, and 5 mM for RT. The values above each line denote the  $d_{001}$  spacing.

### 3.3. FTIR Analyses

For pure AO, the fingerprint region of vibrations was in the range  $1100\text{--}1700\text{ cm}^{-1}$  [25–27]. Thus, the FTIR spectra of the clay minerals were plotted only in this wave number range

(Figure 7). The locations of AO bands after being sorbed on the clay minerals are listed in Table 2. The band locations of AO and  $\text{AOH}^+$  are also listed.

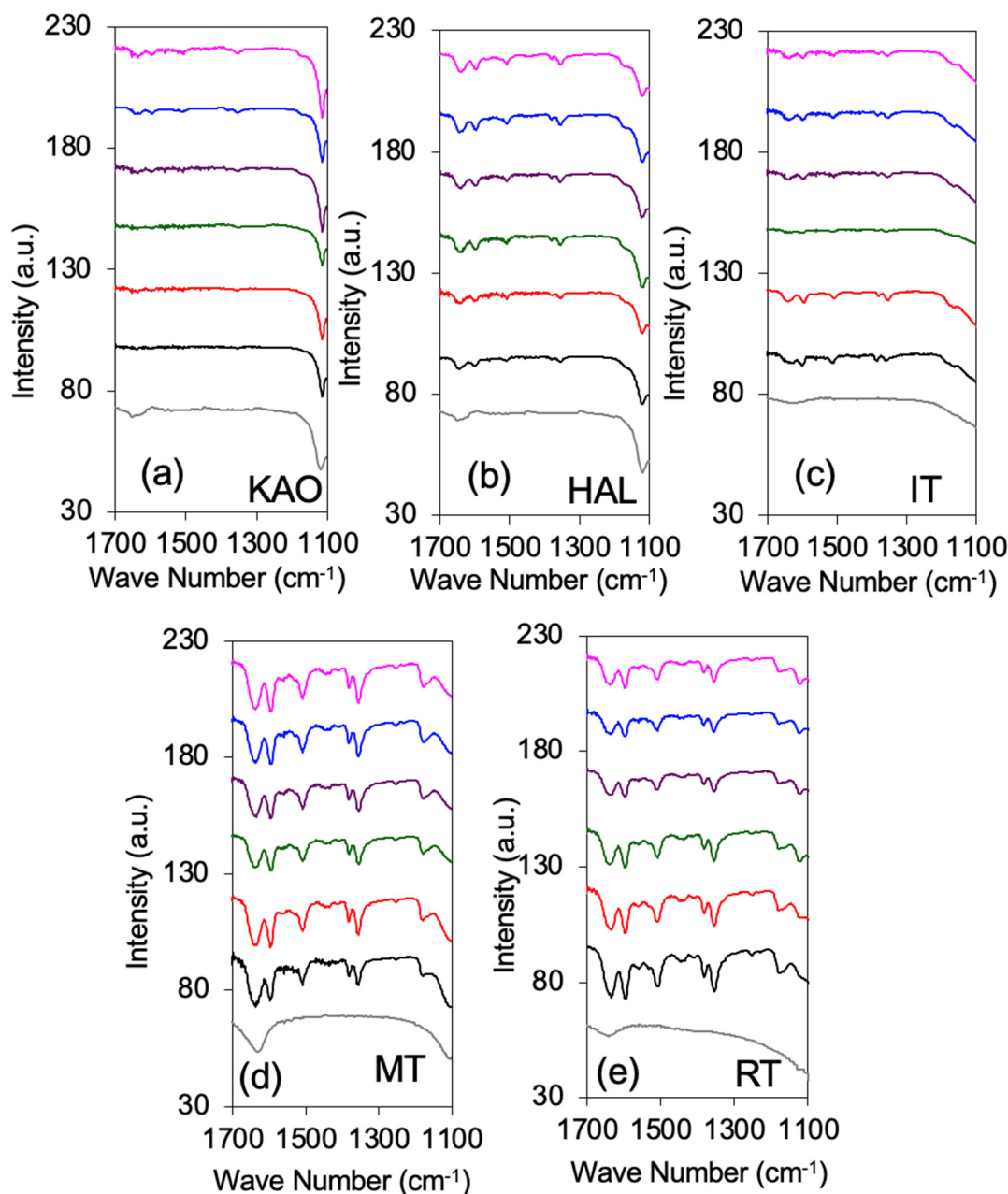


**Figure 7.** FTIR spectra of KAO (a), HAL (b), IT (c), MT (d), and RT (e) showing wavenumbers of 1100–1700  $\text{cm}^{-1}$ . From bottom up, the initial AO concentrations were 0, 0.5, 1, 2, 3, 4, and 5 mM for KAO, HAL, IT, and RT, and 0, 1, 2, 4, 6, 8, and 10 mM for MT. The labels for band position in the figure (e) refer to the locations of original AO bands. See Table 2 for the shift of the bands.

The peak at  $1633\text{ cm}^{-1}$  was ascribed to the C–C stretching band and the scissoring band of N–H of AO and after AO sorption on thermally treated watermelon rinds [28]. It was located at  $1638\text{ cm}^{-1}$  after AO sorption on 2:1 layered clay minerals. The band in the range of  $1573\text{--}1590\text{ cm}^{-1}$  was attributed to the skeletal vibration of the phenyl ring of AO and it shifted to  $1562\text{ cm}^{-1}$  after AO was sorbed onto thermally treated watermelon rinds [28]. In this study, the band was located  $1597\text{--}1599\text{ cm}^{-1}$  after AO sorption on the clay minerals. The intense band at  $1502\text{ cm}^{-1}$  was attributed to an aliphatic  $\sigma_{\text{CN}}$  stretch vibration coupled to aromatic  $\sigma_{\text{CC}}$  stretch motion. The  $\sigma_{\text{CN}}$  contribution was mainly responsible for the large protonation-induced blue shift of  $32\text{ cm}^{-1}$  from  $1474\text{ cm}^{-1}$  [27]. Separately, the sharp peak



at  $1497\text{ cm}^{-1}$  was assigned to the aliphatic CN stretching coupled to the aromatic C=C vibrations [28]. In this study, it was located at  $1508\text{ cm}^{-1}$  after AO sorption on the clay minerals, suggesting participation of the CN in AO sorption. A small peak at  $1501\text{ cm}^{-1}$  appeared after AO sorption onto thermally treated watermelon rinds and was used as confirmation for the existence of  $\text{AOH}^+$  on the surface of the sorbent [28]. Separately, the ring vibration at  $1602\text{ cm}^{-1}$  decreased to  $1598\text{--}1594\text{ cm}^{-1}$  at high AO loading on MT [2] and decreased from  $1600\text{ cm}^{-1}$  to  $1597\text{ cm}^{-1}$  in this study (Table 2). These results further confirmed that the sorbed AO was indeed in a cationic form of  $\text{AOH}^+$  instead of molecular form AO (Table 2). A similar observation was noticed for AO sorption on the thermally treated watermelon rinds [28] and on high-charge MT in an earlier study [7].

The sharp peak at  $1166\text{ cm}^{-1}$  was due to the in-plane C–H and N–H bending of AO and shifted to  $1160\text{ cm}^{-1}$  with much less intensity and sharpness after AO sorption onto thermally treated watermelon rinds [28]. In this study, it was located at  $1165\text{--}1170\text{ cm}^{-1}$  for non-swelling clay minerals and up to  $1180\text{ cm}^{-1}$  for swelling clay minerals after their uptake of AO. The peak at  $919\text{ cm}^{-1}$  was due to the rocking of N–H, which shifted to  $883\text{ cm}^{-1}$  following AO sorption onto thermally treated watermelon rinds; the medium peak at  $696\text{ cm}^{-1}$ , due to N–H twisting, disappeared upon sorption onto thermally treated watermelon rinds [28]. However, these bands could not be resolved due to the strong peak associated with the minerals.

**Table 2.** Band positions and suggested assignments of AO sorption on different types of clay minerals.

Band Assignment <sup>a,b</sup>	Band Position ( $\text{cm}^{-1}$ ) on Different Clay Minerals						
	$\text{AOH}^+$ <sup>a</sup>	AO <sup>c</sup>	KAO	HAL	IT	MT	RT
Ring stretching		1635	-	-	1638	1638	1638
$\sigma_{\text{CC}}$ (8b of ring 1/8b of ring 2)	1603	1592	1599	1599	1597	1597	1597
$\sigma_{\text{CC}}$ (8b of ring 2)/ $\sigma_{\text{CN}}$	1502	1505	1508	1508	1508	1508	1508
$\sigma_{\text{CC}}$ (19b of ring 1)/ $\sigma_{\text{CN}}$ / $\beta_{\text{NH/CH}_3}$ (sym)	1383	1380	-	1381	1383	1381	1383
$\sigma_{\text{CN}}/\beta_{\text{CN}}$	1359	1352	1356	1354	1356	1356	1356
$\beta_{\text{CH}}$ (14 of ring 2)	1167	1170	1170	1167	1165	1179	1180

<sup>a</sup> [25]; <sup>b</sup> [29]; <sup>c</sup> [26].

### 3.4. Molecular Dynamics Simulation

Molecular dynamics simulations were performed under low and high AO sorption levels for all minerals. For KAO, a condensed AO monolayer was formed on the KAO surfaces at the sorption level equivalent to its CEC value, as reviewed along [100] (Figure 8a) and [1] (Figure 8b) directions, and  $\text{Zn}^{2+}$  was not involved in AO sorption (Figure 8). At the AO sorption capacity of  $0.055\text{ mmol/g}$ , the AO bilayer was formed and the co-sorbed  $\text{Zn}^{2+}$  served as a bridging cation, as reviewed along [100] (Figure 9a) and [1] (Figure 9b) directions. HAL often forms nanotubes with the  $\text{SiO}_2$  tetrahedral sheet on the external surface and  $\text{Al}_2\text{O}_3$  octahedral sheet on the inner surface. As such, the external surface is negatively charged while the inner surface is positively charged in a neutral environment [30]. Halloysite often forms nanotubes, due to misfitting of the  $b$  dimensions of the tetrahedral sheet and octahedral sheet, with  $b_{\text{tet}} = 9.164\text{ \AA}$  and  $b_{\text{oct}} = 8.655\text{ \AA}$  [31]. In the simulation, the surface of HAL was treated as flat according to the unit cell parameters of  $a = 5.14(4)\text{ \AA}$ ,  $b = 8.90(4)\text{ \AA}$ ,  $c = 14.9(1)\text{ \AA}$ ,  $\beta = 101.9^\circ$  [32], and  $4a \times 4b$  unit cell parameters were used. With the AO sorption capacity of  $0.12\text{ mmol/g}$  and the CEC value of  $0.115\text{ mmol/g}$ , the sorbed AO molecules only formed a condensed monolayer at the sorption maximum with AO sorption on the negatively charged  $\text{SiO}_2$  tetrahedral sheet, while  $\text{Zn}^{2+}$  was not involved in AO monolayer formation, as reviewed along [100] (Figure 10a) and [1] (Figure 10b) directions. If  $b_{\text{tet}} = 9.164\text{ \AA}$  was used, the AO monolayer density might have been slightly lower. For IL, the molecular dynamics simulation showed monolayer and patchy bilayer AO sorption at the low and high sorption levels (Figure 11). The CEC value was  $0.15\text{ mmol/g}$  for IL, and the AO and AO +  $\text{Zn}^{2+}$  sorption maxima were at  $0.09$  and  $0.16\text{ mmol/g}$ . Co-sorption of  $\text{Zn}^{2+}$  was also noticed.

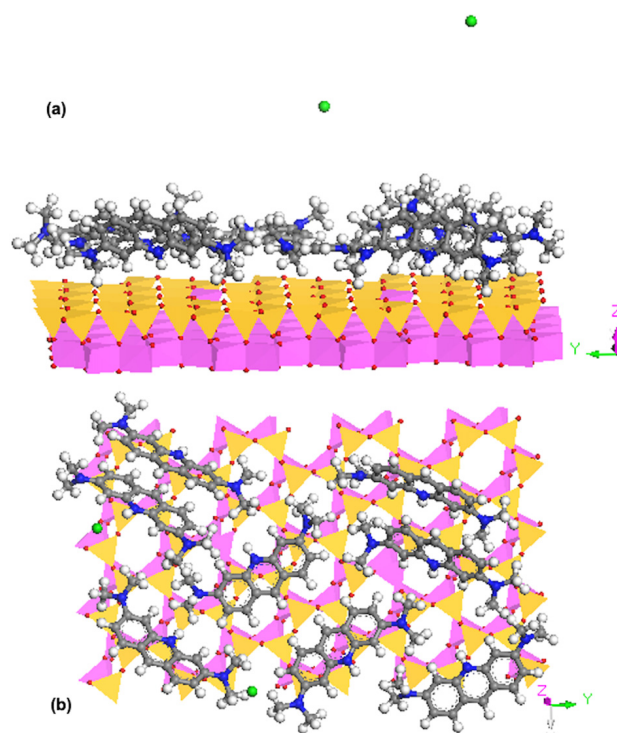


**Figure 8.** Molecular dynamics simulation showing sorbed AO forming a condensed monolayer on KAO at the amount equivalent to its CEC value of 0.03 mmol/g (a,b).  $Zn^{2+}$ : Green.

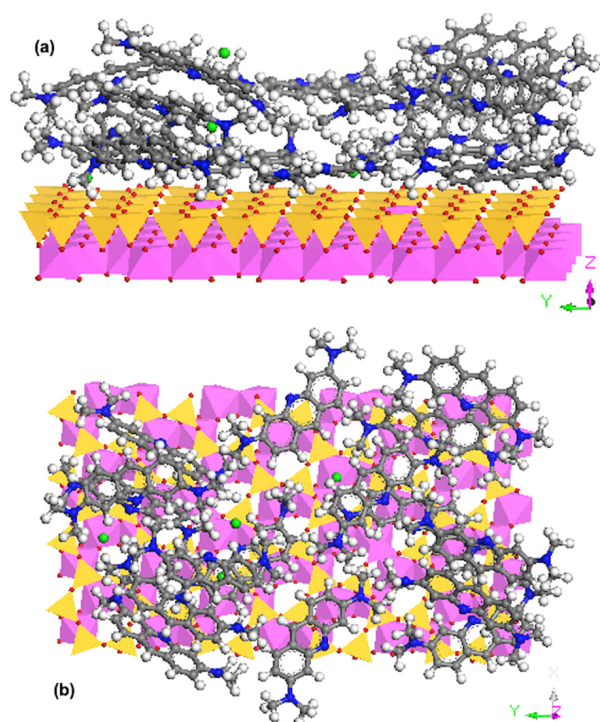


**Figure 9.** Molecular dynamics simulation showing a bilayer configuration on KAO with an AO sorption of 0.055 mmol/g (a) and the influence of  $Zn^{2+}$  (green dots) on AO sorption (b).

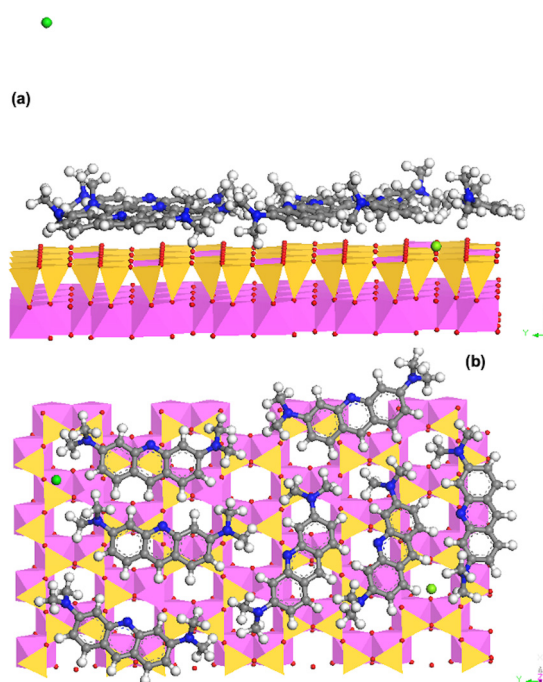


**Figure 10.** Molecular dynamics simulation showing condensed AO monolayer configuration on HAL (a) at the AO sorption capacity (b). Zn: green.

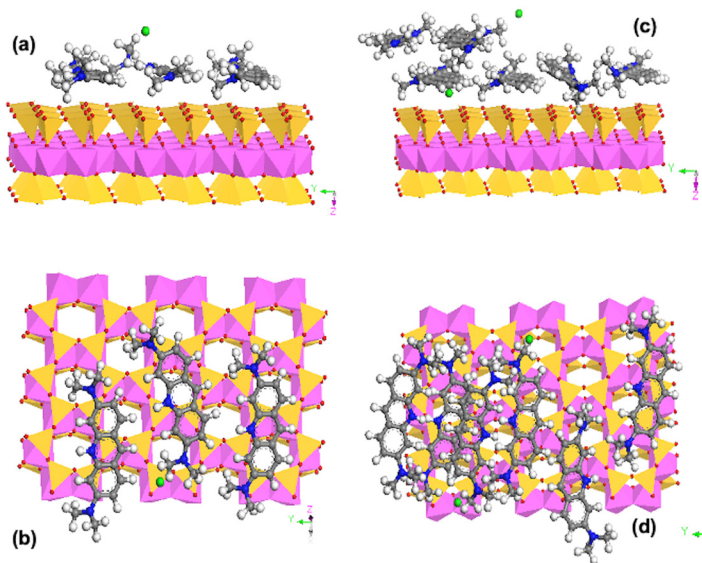


**Figure 11.** Molecular dynamics simulation showing AO configuration on IL at low (a,b) and high (c,d) sorption levels. Zn: green.

With a single monolayer of AO intercalated in the interlayer space of MT, the aromatic rings would be parallel to the aluminosilicate layer, and dimer formation would be anticipated at high AO loading levels, as speculated by Cohen and Yariv [2], as confirmed in the molecular dynamics simulation in this study. For MT, the simulation for low and high loadings resulted in monolayer and bilayer AO intercalation in the expandable interlayer (Figure 12a,b). RT is a regular mixed-layer clay mineral composed of one layer of MT and one layer of IT. Its  $d_{001}$  spacing expansion should come from the MT layer. As the increase in  $d_{001}$  for MT and RT was at the same magnitude, the same AO configuration in the interlayer space of RT and MT would be anticipated. As such, monolayer and bilayer AO intercalation was also found in the interlayer of RT from the simulation results

(Figure 12c,d). Previously, molecular simulations showed dimer and horizontal bilayer formation in the interlayer of MT at low and high sorption levels [6]. The results from this study agree well with previous results of the  $d_{001}$  expansion from 1.38–1.41 nm for AO monolayer intercalation to 1.68–1.71 nm for AO bilayer intercalation into the interlayer of low-charged SWy-2 Na-MT [6]. Again, no  $\text{Zn}^{2+}$  was involved in AO monolayer interaction; however,  $\text{Zn}^{2+}$  was co-sorbed in the interlayer of MT or participated in AO bilayer formation, which is a new finding not previously reported.

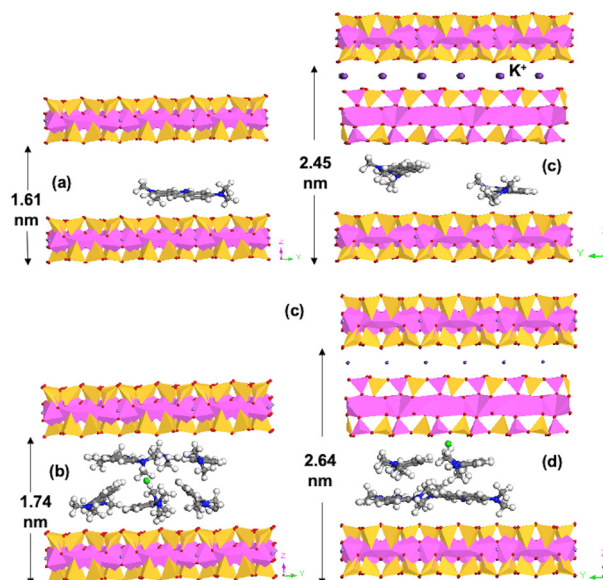


**Figure 12.** Molecular dynamics simulation showing AO intercalation in the interlayer of MT (a,b) and RT (c,d) under monolayer (a,c) and bilayer (b,d) configurations. Zn: green.

Three types of metachromasy were considered after AO sorption on smectites, which are  $\pi$  interactions between the O plane of the mineral and the aromatic ring of AO, dimerization of AO in the interparticle space, and sorption of dimeric and polymeric cations on the surfaces of the tactoids [24]. The molecular dynamics simulation results also showed these types of interactions (Figure 12b,d). The  $\text{Zn}^{2+}$  in the dimeric or bilayer AO sorption in the interlayer of MT and RT showed bridging of the AO bilayer in the MT interlayer but no association with AO in the RT interlayer, suggesting that  $\text{Zn}^{2+}$  might just be competing against AO for the sorption sites.

The dynamics of the simulation for AO and AO +  $\text{Zn}^{2+}$  sorption on the clay minerals under low and high sorption levels were recorded as movies and can be found in Supplementary Videos S1–S9. For KAO under high AO loading (S2),  $\text{Zn}^{2+}$  had a tendency to accumulate on the surface instead of staying away from the surface under monolayer coverage (S1). Similar simulation results were found for IL (S5 vs. S4). For HAL under a high AO loading level, some  $\text{Zn}^{2+}$  accumulated on the surface, whereas some stayed away from the surface (S3). For MT and RT, under low AO loading levels,  $\text{Zn}^{2+}$  did not sorb onto the mineral surfaces or at the interlayer. Thus, no  $\text{Zn}^{2+}$  was added to the simulation (S6 and S8). For MT, under higher AO loading level, it seemed that  $\text{Zn}^{2+}$  played a bridging role (S7), similar to the results in Figure 12b. However, for RT, under high AO loading level,  $\text{Zn}^{2+}$  had a tendency to accumulate on the interlayer faces (S9).

#### 4. Discussion

AO may form dimers at high concentrations with a dimerization constant  $K_D$  calculated as

$$K_D = \frac{[D]}{[M]^2} \quad (3)$$



where  $[D]$  and  $[M]$  are the concentrations of AO dimers and monomers, respectively.  $K_D$  was listed as  $2 \times 10^{-6}$  [33]. In contrast, most  $K_D$  values in the literature were calculated as  $1.05 \times 10^4 \text{ M}^{-1}$  [17],  $3.6 \times 10^5 \text{ M}^{-1}$  [34], or  $1.6 \times 10^4 \text{ M}^{-1}$  [35], and a  $\log K_D$  of 6 was also reported for AO concentrations of 1 to 10  $\mu\text{M}$  [36]. Moreover, Costantino [37] listed  $K_D$  values from four different sources ranging from 8500–22,000  $\text{M}^{-1}$ . If the low value of 8500  $\text{M}^{-1}$  was used, at the low initial AO concentration of 0.5 mmol/L in the isotherm study, the monomer and dimer concentrations would be 0.14 and 0.18 mmol/L, while, at the high initial AO concentration of 5 mmol/L, the monomer and dimer concentrations would be 0.51 and 2.24 mmol/L, calculated using Equation (3). On the other hand, if the high value of 100,000  $\text{M}^{-1}$  was used, at the low initial AO concentration of 0.5 mmol/L the monomer and dimer concentrations would be 0.05 and 0.23 mmol/L, and at the high initial AO concentration of 5 mmol/L, the monomer and dimer concentrations would be 0.16 and 2.42 mmol/L. These results confirmed that AO dimers were the dominant species in the initial solutions of AO before the equilibrium study. With the 0.5 mmol/L input concentration, at equilibrium, the AO concentrations were 0.42, 0.19, and 0.25 mmol/L for KAO, HAL, and IL. Under these concentrations, the monomer and dimer concentrations would be 0.04 and 0.19, 0.03 and 0.18, and 0.03 and 0.11 mmol/L, respectively. Thus, for the non-swelling clay minerals, the dimer–monomer concentration ratio ranged from 4:1 to 6:1. For swelling clay minerals, the equilibrium AO concentrations were 0 mmol/L under low initial concentrations. However, the equilibrium concentrations were 0.4 and 0.6 mmol/L for the lowest detectable equilibrium concentrations, under which the AO monomer and dimer concentrations were 0.04 and 0.18 mmol/L and 0.05 and 0.27 mmol/L; nevertheless, the ratio of dimer–monomer concentration was about 5:1. Thus, significant dimer sorption should occur even under low AO loading levels. On the other hand, due to the large SSA, the surface reconfiguration under low AO input would result in breakdown of dimers into monomer, leading to monolayer formation under low AO loading levels. Under high AO loading levels, the SSA became the limiting factor. Thus, dimer or bilayer formation of AO is inevitable. On the other hand, the observed dimerizing order as affected by the types of salts in solution is  $\text{KBr} > \text{KCl} \approx \text{NaCl} > \text{LiCl} > \text{MgCl}_2$  [33]. However, the concentrations of these cations in solution due to desorption in this study were much lower; thus, they may not be the major reason for the formation of AO dimers on the surface or in the interlayer of the clay minerals. If the above order is extended to  $\text{ZnCl}_2$ , it would be on the order of  $\text{MgCl}_2$  or even lower. Thus, the influence of presenting  $\text{Zn}^{2+}$  on enhanced dimerization of AO should be minimal.

Sorption of AO on clay minerals was previously attributed to cation exchange [24]. However, there was no mention of the effect of co-presenting cations on AO sorption. In this study, it was noticed that the dominant function of co-presenting  $\text{Zn}^{2+}$  might be a competing effect against AO sorption, although a bridging effect for the formation of AO dimer or bilayer might also play some role. In addition, the AO sorption was limited to the external surface of the non-swelling clay minerals. Thus, the SSA and CEC played an important role. For swelling clay minerals, not only the SSA, but also the interlayer spaces are host sites for cationic dyes. Regardless, in the true mechanism of  $\text{Zn}^{2+}$  on AO sorption, the co-presenting  $\text{Zn}^{2+}$  might have a small negative effect when using clay minerals for the removal of cationic dyes from water.

## 5. Conclusions

In this study, the sorption of AO, a fluorescence dye used in DNA analyses, on non-swelling and swelling clay minerals was investigated. It was found that the uptake of AO on the minerals correlated well to the CEC values of the minerals, suggesting that cation exchange played a significant role in AO sorption on clay minerals. In addition, AO sorption was limited to the external surfaces of non-swelling clay minerals, while both external surfaces and interlayer spaces were responsible for AO sorption on swelling clay minerals. Stoichiometric desorption of exchangeable cations due to sorption of AO or  $\text{AO} + \text{Zn}^{2+}$  also suggested a cation exchange mechanism. In addition, the results from



this study demonstrated the competitive effect of co-presenting cation  $\text{Zn}^{2+}$  toward  $\text{AOH}^+$  sorption. However, per equivalent, at the sorption capacity, the amount of AO sorbed was about twice the amount of  $\text{Zn}^{2+}$  sorbed per charge, suggesting that the organic cations have a higher affinity for negatively charged mineral surfaces in comparison to the divalent inorganic cation  $\text{Zn}^{2+}$ . The findings in this study strongly suggest that Earth materials, particularly clay minerals with a high specific surface area and large cation exchange capacity, are good candidates for the removal of cationic organic dyes from solution, and that the competition effect from co-presenting inorganic cations is present, but should not be much of a concern.

**Supplementary Materials:** The following supporting information can be downloaded at: <https://www.mdpi.com/article/10.3390/cryst12010118/s1>. Videos S1–S9. Movie clips for AO and  $\text{Zn}^{2+}$  sorption on KAO at low (S1) and high (S2), on HAL at high (S3), on IL at low (S4) and high (S5), on MT at low (S6) and high (S7), and on RT at low (S8) and high (S9) loading.

**Author Contributions:** Conceptualization, W.-T.J. and Z.L.; methodology, Z.L.; software, X.W.; validation, Z.L., W.-T.J. and L.A.; formal analysis, Y.T., H.J.T. and J.B.; investigation, Y.T.; resources, Z.L.; data curation, Z.L., J.B. and H.J.T.; writing—original draft preparation, Z.L.; writing—review and editing, W.-T.J.; visualization, Z.L. and X.W.; supervision, Z.L. and W.-T.J.; project administration, Z.L. and W.-T.J.; funding acquisition, Z.L. and W.-T.J. All authors have read and agreed to the published version of the manuscript.

**Funding:** This research was funded by a SPARK grant provided from WiSys. Ref. No. T210025.

**Institutional Review Board Statement:** Not applicable.

**Informed Consent Statement:** Patent consent was waived due to the materials used being raw materials.

**Data Availability Statement:** Upon request.

**Conflicts of Interest:** The authors declare no conflict of interest.

## References

1. Darzynkiewicz, Z. Differential staining of DNA and RNA in intact cells and isolated cell nuclei with acridine orange. *Methods Cell Biol.* **1990**, *33*, 285–298.
2. Cohen, R.; Yariv, S. Metachromasy in clay minerals. Sorption of acridine orange by montmorillonite. *J. Chem. Soc. Faraday Trans. 1 Phys. Chem. Condens. Phases* **1984**, *80*, 1705–1715. [\[CrossRef\]](#)
3. Garfinkel-Shweky, D.; Yariv, S. Metachromasy in clay dye systems: The adsorption of acridine- orange by Na-saponite. *Clay Min.* **1997**, *32*, 653–663. [\[CrossRef\]](#)
4. Garfinkel-Shweky, D.; Yariv, S. Metachromasy in clay dye systems: The adsorption of acridine orange by Na-beidellite. *Clay Min.* **1999**, *34*, 459–467. [\[CrossRef\]](#)
5. Chattopadhyay, S.; Traina, S.J. Spectroscopic study of sorption of nitrogen heterocyclic compounds on phyllosilicates. *Langmuir* **1999**, *15*, 1634–1639. [\[CrossRef\]](#)
6. Lv, G.; Li, Z.; Jiang, W.T.; Chang, P.H.; Jean, J.S.; Lin, K.H. Mechanism of acridine orange removal from water by low-charge swelling clays. *Chem. Eng. J.* **2011**, *174*, 603–611. [\[CrossRef\]](#)
7. Lv, G.; Wu, L.; Liao, L.; Jiang, W.T.; Li, Z. Intercalation and configurations of organic dye acridine orange in a high-charge montmorillonite as influenced by dye loading, Desal. *Water Treat.* **2014**, *52*, 7323–7331. [\[CrossRef\]](#)
8. Khelifi, S.; Mallah, B.; Ayadi, M.T.; Oueslatic, M.H.; Sbihi, H.M.; Ayari, F. Performance of a local clay deposit in adsorptive and photochemical removal of Acridine Orange dye and DNA indicator from wastewater. *Desal. Water Treat.* **2020**, *206*, 396–406. [\[CrossRef\]](#)
9. Bhattacharjee, J.; Hussain, S.A.; Bhattacharjee, D. Control of H-dimer formation of acridine orange using nano clay platelets. *Spectrochim. Acta Part A* **2013**, *116*, 148–153. [\[CrossRef\]](#) [\[PubMed\]](#)
10. Kadhim, B.A.; Muhmood, A.A.; Jabbar, B.S.; Mahdi, L.H. Study the kinetic of Acridine orange dye adsorption by ZnO/GO nanocomposite. *J. Iraqi Al-Khwarizmi Soc.* **2020**, *4*, 85–94.
11. Khan, S.A.; Khan, S.B.; Asiri, A.M. Layered double hydroxide of Cd-Al/C for the mineralization and de-coloration of dyes in solar and visible light exposure. *Sci. Rep.* **2016**, *6*, 35107. [\[CrossRef\]](#) [\[PubMed\]](#)
12. Qadri, S.; Ganoie, A.; Haik, Y. Removal and recovery of acridine orange from solutions by use of magnetic nanoparticles. *J. Hazard. Mater.* **2009**, *169*, 318–323. [\[CrossRef\]](#) [\[PubMed\]](#)
13. Zbair, M.; Anfar, Z.; Ahsaine, H.A.; El Alem, N.; Ezahri, M. Acridine orange adsorption by zinc oxide/almond shell activated carbon composite: Operational factors, mechanism and performance optimization using central composite design and surface modeling. *J. Environ. Manag.* **2018**, *206*, 383–397. [\[CrossRef\]](#)

14. Jiang, W.T.; Tsai, Y.; Wang, X.; Li, Z. Enhanced fluorescence effect of acridine orange sorbed on 2:1 layered clay minerals. *Appl. Clay Sci.* **2020**, *189*, 105534. [CrossRef]
15. Jiang, W.T.; Tsai, Y.; Wang, X.; Li, Z. Optimization of acridine orange loading on 1:1 layered clay minerals for fluorescence enhancement. *J. Ind. Eng. Chem.* **2020**, *90*, 407–418. [CrossRef]
16. Falcone, R.D.; Correa, N.M.; Biasutti, M.A.; Silber, J.J. Acid–base and aggregation processes of acridine orange base in n-heptane/AOT/water reverse micelles. *Langmuir* **2002**, *18*, 2039–2047. [CrossRef]
17. Lamm, M.E.; Neville, D.M., Jr. The dimer spectrum of acridine orange hydrochloride. *J. Phys. Chem.* **1965**, *69*, 3872–3877. [CrossRef]
18. Robinson, B.H.; Löffler, A.; Schwarz, G. Thermodynamic behaviour of acridine orange in solution. Model system for studying stacking and charge-effects on self-aggregation. *J. Chem. Soc. Faraday Trans. 1 Phys. Chem. Condens. Phases* **1973**, *69*, 56–69. [CrossRef]
19. Borden, D.; Giese, R.F. Baseline studies of the clay minerals society source clays: Cation exchange capacity measurements by the ammonia-electrode method. *Clays Clay Miner.* **2001**, *49*, 444–445. [CrossRef]
20. Jiang, W.T.; Chang, P.H.; Tsai, Y.; Li, Z. Halloysite nanotubes as a carrier for the uptake of selected pharmaceuticals. *Micropor. Mesopor. Mater.* **2016**, *220*, 298–307. [CrossRef]
21. Jaynes, W.F.; Bigham, J.M. Multiple cation-exchange capacity measurements on standard clays using a commercial mechanical extractor. *Clays Clay Miner.* **1986**, *34*, 93–98. [CrossRef]
22. Hong, H.; Zhang, X.; Wan, M.; Hou, Y.; Du, D. Morphological characteristics of (K, Na)-rectorite from Zhongxiang rectorite deposit, Hubei, central China. *J. China Univ. Geosci.* **2008**, *19*, 38–46. [CrossRef]
23. Środoń, J.; MaCarty, D.K. Surface area and layer charge of smectite from CEC and EGME/H<sub>2</sub>O-retention measurements. *Clays Clay Miner.* **2008**, *56*, 155–174. [CrossRef]
24. Yariv, S.; Vonmoos, M.M.; Kahr, G.; Rub, A. Thermal analytic study of the adsorption of acridine orange by smectite minerals. *J. Thermal. Anal.* **1989**, *35*, 1997–2008. [CrossRef]
25. Zimmermann, F.; Hossenfelder, B.; Paanitz, J.-C.; Wokaun, A. SERRS Study of acridine orange and its binding to DNA strands. *J. Phys. Chem.* **1994**, *98*, 12796–12804. [CrossRef]
26. Nafisi, S.; Saboury, A.A.; Keramat, N.; Neault, J.-F.; Tajmir-Riahi, H.-A. Stability and structural features of DNA intercalation with ethidium bromide, acridine orange and methylene blue. *J. Molec. Struct.* **2007**, *827*, 35–43. [CrossRef]
27. Lagutschenkov, A.; Dopfer, O. Infrared spectrum of a protonated fluorescence dye: Acridine orange. *J. Molec. Spectrosc.* **2011**, *268*, 66–77. [CrossRef]
28. El-Shafie, A.S.; Hassan, S.S.; Akther, N.; El-Azazy, M. Watermelon rinds as cost-efficient adsorbent for acridine orange: A response surface methodological approach. *Environ. Sci. Pollut. Res.* **2021**, 1–20. [CrossRef]
29. Agravat, S.; Jain, V.; Oza, A.T. Vibrational spectra of CT complexes of acridine orange. *Indian J. Chem.* **2008**, *47A*, 341–347.
30. Abdullayev, E.; Lvov, Y. Halloysite for controllable loading and release. In *Developments in Clay Science*; Elsevier: Amsterdam, The Netherlands, 2016; Volume 7, pp. 554–605.
31. Singh, B. Why does halloysite roll?—A new model. *Clays Clay Miner.* **1996**, *44*, 191–196. [CrossRef]
32. Halloysite-7Å. Available online: <https://www.mindat.org/min-10408.html> (accessed on 14 December 2021).
33. Moulik, S.P.; Ghosh, S.; Das, A.R. Dimerization of acridine orange monohydrochloride in the presence of LiCl, NaCl, KCl, KBr, KI, Me<sub>4</sub>NI & MgCb & the co-solvents glucose, formamide, sucrose, urea, methanol, ethanol, ethylene glycol, propylene glycol, dioxane & isopropanol. *Indian J. Chem.* **1976**, *14A*, 306–310.
34. Ghosh, S.; Moulik, S.P.; Das, A.R. Spectrophotometric investigation on the interaction of acridine orange with methylene blue, phenosafranin, and disulphine blue in aqueous medium. *Can. J. Chem.* **1981**, *59*, 2449–2456. [CrossRef]
35. Murakami, K.; Mizuguchi, K.; Kubota, Y.; Fujisaki, Y. Equilibrium and kinetic studies of the dimerization of acridine orange and its 10-alkyl derivatives. *Bull. Chem. Soc. Jpn.* **1986**, *59*, 3393–3397. [CrossRef]
36. Ghasemi, J.; Niazi, A.; Nikrahi, A. Spectroscopic thermodynamic study of the dimerization reaction of acridine orange by chemometrics analysis at different ionic strengths. *Anal. Chem. Indian J.* **2006**, *2*, 65–72.
37. Costantino, L.; Guarino, G.; Ortona, O.; Vitagliano, V. Acridine orange association equilibrium in aqueous solution. *J. Chem. Engineer. Data* **1984**, *29*, 62–66. [CrossRef]